Neurobiology:

An Engineered Glutamate-gated Chloride (GluCl) Channel for Sensitive, Consistent Neuronal Silencing by Ivermectin

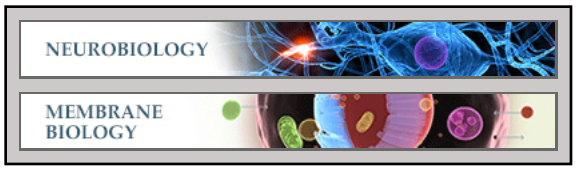

Shawnalea J. Frazier, Bruce N. Cohen and Henry A. Lester

J. Biol. Chem. 2013, 288:21029-21042.
doi: 10.1074/jbc.M112.423921 originally published online May 29, 2013

THE JOURNAL OF BIOLOGICAL CHEMISTRY VOL. 288, NO. 29, pp. 21029–21042, July 19, 2013

An Engineered Glutamate-gated Chloride (GluCl) Channel for Sensitive, Consistent Neuronal Silencing by Ivermectin*

Received for publication, September 28, 2012, and in revised form, May 27, 2013 Published, JBC Papers in Press, May 29, 2013, DOI 10.1074/jbc.M112.423921

Shawnalea J. Frazier[‡§], **Bruce N. Cohen**[§], **and Henry A. Lester**[§1]

From the [‡]*Biochemistry and Molecular Biophysics Option and the* [§]*Division of Biology, California Institute of Technology, Pasadena, California 91125*

Background: Ivermectin (IVM) silences activity in neurons expressing glutamate-gated chloride channels (GluCl).
Results: Rational point mutations in GluCl robustly increase IVM-induced conductance and reduce the variability of spike suppression in cultured neurons.
Conclusion: The newly engineered receptor improves heteromeric receptor expression and sensitivity to IVM.
Significance: GluClv2.0 is an improved tool for IVM-induced silencing.

A modified invertebrate glutamate-gated Cl^- channel (GluCl $\alpha\beta$) was previously employed to allow pharmacologically induced silencing of electrical activity in CNS neurons upon exposure to the anthelmintic drug ivermectin (IVM). Usefulness of the previous receptor was limited by 1) the high concentration of IVM necessary to elicit a consistent silencing phenotype, raising concern about potential side effects, and 2) the variable extent of neuronal spike suppression, due to variations in the co-expression levels of the fluorescent protein-tagged α and β subunits. To address these issues, mutant receptors generated via rational protein engineering strategies were examined for improvement. Introduction of a gain-of-function mutation (L9′F) in the second transmembrane domain of the α subunit appears to facilitate β subunit incorporation and substantially increase heteromeric GluCl $\alpha\beta$ sensitivity to IVM. Removal of an arginine-based endoplasmic reticulum retention motif (RSR mutated to AAA) from the intracellular loop of the β subunit further promotes heteromeric expression at the plasma membrane possibly by preventing endoplasmic reticulum-associated degradation of the β subunit rather than simply reducing endoplasmic reticulum retention. A monomeric XFP (mXFP) mutation that prevents fluorescent protein dimerization complements the mutant channel effects. Expression of the newly engineered GluCl opt α-mXFP L9′F + opt β-mXFP Y182F RSR_AAA receptor in dissociated neuronal cultures markedly increases conductance and reduces variability in spike suppression at 1 nM IVM. This receptor, named "GluClv2.0," is an improved tool for IVM-induced silencing.

The development of optogenetic and orthogonal pharmacogenetic techniques to manipulate neuronal activity has become an important sector of neuroscience. These tools enable mapping of neuronal connectivity and are essential for assigning functional roles to particular cell types and determining their contribution to perception or behavior. We previously used a heteromeric glutamate-gated chloride channel (GluCl $\alpha\beta$) cloned from the invertebrate species *Caenorhabditis elegans* to silence mammalian neuronal activity *in vivo* (1). Activation of GluCl channels by the anthelmintic drug ivermectin (IVM)[2] elicits a chloride conductance that drives the membrane potential toward the Nernst potential of Cl^- (E_{Cl}), preventing action potential generation for effective neuronal silencing (2).

Prior to its implementation as a silencing tool, the *C. elegans* GluCl receptor underwent several genetic modifications. First, it was rendered insensitive to its native ligand glutamate by a single point mutation (Y182F) in the β subunit (3). Second, the DNA sequences of the invertebrate α and β subunits were codon-optimized (opt α and opt β) to achieve greater protein expression levels in mammalian cells (4). Third, fluorescent protein tags (YFP and CFP; often noted as XFP) were inserted into the large intracellular loop of each subunit to allow for direct visualization of protein expression (3). We refer to this GluCl opt α-XFP + opt β-XFP Y182F receptor throughout this paper as "GluCl version 1.0" or simply "GluClv1.0."

The GluCl/IVM method was the first to show neuronal silencing induced by a systemically administered drug in awake, behaving animals (1). IVM administration caused unidirectional rotational behavior in mice expressing GluClv1.0 in the unilateral striatum, indicating that striatal neurons were silenced. The rotational behavior was observed within hours of induction and was fully reversed within days, allowing multiple cycles of silencing and recovery to be performed on a single animal. Selective and reversible silencing was achieved without measurable toxicity to either individual neurons or the animal as a whole. However, the dose of IVM required to elicit a consistent silencing phenotype (5–10 mg/kg) (1) was higher than that routinely used to treat mice with parasitic infections (0.2 mg/kg) (5), presumably because engineered silencing requires CNS penetration. The required concentrations were in the

* This work was supported, in whole or in part, by National Institutes of Health Grants NS034407, EY018502, and MH088550. This work was also supported by the McKnight Foundation.
[1] To whom correspondence should be addressed: Division of Biology, MC 156-29, California Institute of Technology, 1200 E. California Blvd., Pasadena, CA 91125. Tel.: 626-395-4946; Fax: 626-564-8709; E-mail: lester@caltech.edu.

[2] The abbreviations used are: IVM, ivermectin; GluCl, glutamate-gated chloride channel; HEK, human embryonic kidney; ER, endoplasmic reticulum; TIRF, total internal reflection fluorescence; nMDP, normalized mean deviation product; CFP, cyan fluorescent protein; XFP, YFP and CFP; mYFP and mXFP, monomeric YFP and XFP, respectively.

range to raise concern about potential side effects because IVM is known to activate (or potentiate) other ligand-gated ion channels in the CNS, although it does so much less potently than GluCl (6–9). In addition, the silencing phenotype displayed a bimodal distribution that correlated with both the extent of viral infection (*i.e.* the volume of striatum expressing GluCl $\alpha\beta$) and the extent of spike suppression (*i.e.* individual neurons showing either full, partial, or no inhibition), which further correlated with the co-expression levels of α and β subunits.

GluClv1.0 was thus a candidate for rational protein optimization that would 1) alleviate the concern of off-target side effects and 2) avoid suboptimal spike inhibition. Toward aim 1, we screened heteromeric GluCl $\alpha\beta$ for increased sensitivity to IVM by introducing channel gating mutations in the second transmembrane domain of the α subunit. To employ IVM effectively as an orthogonal silencing tool, however, we had to reinstate glutamate insensitivity (by reintroduction of the βY182F mutation) to this hypersensitive mutant receptor. For aim 2, we suspected that inadequate surface expression of the β subunit was responsible for the variability in spike suppression. To improve heteromeric receptor expression at the plasma membrane, putative trafficking determinants of the β subunit were mutated. An additional mutation designed to prevent fluorescent protein dimerization appeared to enhance heteromeric subunit assembly. Altogether, *in vitro* silencing experiments unequivocally show that the resulting mutant receptor is a more sensitive and less variable GluCl/IVM silencing tool.

EXPERIMENTAL PROCEDURES

Site-directed Mutagenesis—Codon optimized sequences of the *C. elegans* GluCl channel, including optGluCl αWT, optGluCl βWT, optGluCl α-XFP, and optGluCl β-XFP (4), cloned into plasmid vector pcDNA3.1/V5-His TOPO (catalog no. K4800-01, Invitrogen) were used in this study. Fluorescent protein insertions (XFP) include enhanced yellow (YFP) and cyan (CFP) variants and are located in the M3-M4 loop (3). For convenience, the "opt" nomenclature is omitted throughout most of this paper. Mutations were made using the QuikChange II XL site-directed mutagenesis kit (catalog no. 200522, Agilent Technologies) and PfuTurbo DNA polymerase (catalog no. 600250, Agilent Technologies). Forward and reverse primers for the (α)L9′F mutation were 5′-CC CTG GGC GTG ACC ACC CTG xxx AC-3′ and 5′-GC GGA CTG AGC GGT CAT GGT xxx CA-3′, where "xxx" delineates the mutated Leu9′ codon. Leu9′ mutations included Ile, Phe, Val, Ser, Thr, Ala, and Gly. Additional mutations in this study were generated using the following forward and reverse primers (mutant codon is italicized in the forward primer): 5′-AC TTC GAC CTG GTG TCC *TTC* GCC CAC ACC-3′ and 5′-GGT GTG GGC GAA GGA CAC CAG GTC GAA GT-3′ for the (β)Y182F mutation; 5′-TAC CTG AGC TAC CAG TCC *AAG* CTG AGC AAA GAC CCC AAC-3′ and 5′-GTT GGG GTC TTT GCT CAG CTT GGA CTG GTA GCT CAG GTA-3′ for the monomeric YFP A206K mutation; 5′-TG CGC CAG AAC GAC *GCC GCC GCC* GAG AAG GCG GCC C-3′ and 5′-G GGC CGC CTT CTC GGC GGC GGC GTC GTT CTG GCG CA-3′ for the (β)RSR_AAA mutation; 5′-CG GCC CGC AAG GCC CAG *GCA GCC GCC* GAG AAG CTG GAG ATG G-3′ and 5′-C CAT CTC CAG CTT CTC GGC GGC TGC CTG GGC CTT GCG GGC CG-3′ for the (β)RRR_AAA mutation. A C-terminal V5 tag was added to α and β subunits by mutating the stop codon using the following primers: 5′-G CAG AAC GTT CTG TTC *GGA* GCT AGC AAG GGC AA-3′ and 5′-TT GCC CTT GCT AGC TCC GAA CAG AAC GTT CTG C-3′ for the α subunit; 5′-CC GAG TCC CTG GTG *TTG* GCT AGC AAG G-3′ and 5′-C CTT GCT AGC CAA CAC CAG GGA CTC GG-3′ for the β subunit. All mutations were verified by DNA sequencing.

Cell Culture—Human embryonic kidney 293 (HEK293) cells were purchased from ATCC (catalog no. CRL-1573). Cells were cultured in Dulbecco's modified Eagle's medium (DMEM; catalog no. 11965, Invitrogen) supplemented with 10% FBS (catalog no. 26140, Invitrogen), 100 units/ml penicillin, 100 μg/ml streptomycin (catalog no. 15140, Invitrogen), and 1 mM sodium pyruvate (catalog no. 11360, Invitrogen) and maintained at 37 °C and 5% CO_2 in a humidified incubator. Cells were passaged when confluent at a subcultivation ratio of 1:5 or 1:10 every 3–4 days. For FlexStation assays, HEK293 cells were plated at 20,000 cells/well, with a plating volume of 100 μl/well, in a black-sided/clear-bottomed 96-well imaging plate (catalog no. 353219, BD Falcon). For transfection, 16 μg of total DNA in 750 μl of DMEM was mixed with 30 μl of ExpressFect in 750 μl DMEM, preincubated for 20 min, and then added at 15 μl/well to cells containing 100 μl of fresh culture medium. Transfection mixes were removed from cultures following a 4–6-h incubation period at 37 °C/5% CO_2 and replaced with fresh culture medium. For total internal reflection fluorescence (TIRF) imaging, HEK293 cells were plated on 35-mm glass bottom culture dishes (catalog no. P35G-1.5-10-C, MatTEK) at 50,000 cells/dish. Cells were transfected with 1 μg of DNA in 100 μl of DMEM plus 4 μl of ExpressFect (catalog no. E2650, Denville Scientific) in 100 μl of DMEM that was preincubated for 20 min before adding to culture dishes containing 2 ml of fresh culture medium. The transfection mix was removed after 4–6 h and replaced with fresh culture medium. For all experiments, HEK293 cells were transfected 24 h after plating and assayed 48 h after transfection.

Hippocampal neurons were obtained from day 18 Wistar rat embryos (10) and plated at a density of 40,000 cells/dish on 35-mm glass bottom culture dishes coated with poly-DL-lysine (catalog no. P9011, Sigma). Neurons were cultured in Neurobasal medium (catalog no. 21103-049, Invitrogen) containing 2% B27 (catalog no. 17504-044, Invitrogen) and 0.5 mM Glutamax (catalog no. 35050, Invitrogen). Medium was supplemented with 5% equine serum (catalog no. SH30074, Hyclone) during plating. Cultures were maintained at 37 °C and 5% CO_2 in a humidified incubator with a 50% medium exchange once per week. For imaging experiments, neurons were treated with 1 μM cytosine arabinoside (catalog no. C1768, Sigma) on culture day 10, followed by a 100% medium change the next day. Cultures used for electrophysiological experiments were not treated with cytosine arabinoside. Neurons were transiently transfected after 13–14 days in culture and assayed 24 h later. Transfections were prepared using 4 μg of plasmid DNA with 20 μg of Nupherin-neuron (catalog no. SE-225, BIOMOL) and

10 μl of Lipofectamine 2000 (catalog no. 11668-019, Invitrogen) diluted separately in 400 μl of Neurobasal without phenol red (catalog no. 12348-017, Invitrogen). The diluted reagents were preincubated separately at room temperature for 15 min and then combined and incubated for another 45 min. An 800-μl volume of conditioned medium was then removed from the neuronal culture dish and replaced with the 800-μl transfection mix. After incubating cultures for 1 h at 37 °C/5% CO_2, an 800-μl volume was removed from the dish and replaced with the original 800 μl of conditioned medium.

Fluorescent Membrane Potential Measurements—Fluorescent membrane potential assays were performed using the FlexStation 3 multimode benchtop microplate reader and the BLUE formulation kit (catalog no. R8042, Molecular Devices). Dye loading buffer was prepared according to the instructions of the manufacturer. To perform the assay, culture medium was removed from the cells and replaced with 50 μl of DMEM. Cells were then loaded with 50 μl of blue dye loading buffer and incubated for 40 min at 37 °C/5% CO_2. Fluorescence was measured at ambient temperature using the "Low PMT" setting of the FlexStation 3 operated by SoftMax Pro Data Acquisition and Analysis Software. Excitation and emission wavelengths were set at 530 and 565 nm, respectively. The emission cut-off was 550 nm. Other FlexStation parameters included a pipette dispensing height of 230 μl for a 300-μl volume well, an initial well volume of 100 μl, a transfer volume of 50 μl (therefore, drug concentrations were prepared three times), and a transfer rate setting of 2, corresponding to ~31 μl/s. Ivermectin concentrations for the FlexStation assay were prepared as 1:10 serial dilutions of 10, 5, and 2 μM using a 1× commercial stock of Hanks' balanced salt solution (without phenol red; catalog no. 14025, Invitrogen) with 20 mM HEPES, pH 7.4, containing 0.1% DMSO.

Electrophysiology—We used an Axopatch 200A amplifier equipped with a CV201 headstage and Digidata 1200 series interface operated by Clampex version 9.2 software (Axon Instruments) to obtain electrophysiological recordings from neurons in whole-cell current clamp mode. Stepwise square current pulses (−100 to 250 pA, 25-pA increments) were used to generate action potentials. Data were sampled at 50 kHz and low pass-filtered at 5 kHz. Neurons were superfused (or incubated) with artificial cerebrospinal fluid composed of 110 mM NaCl, 5.4 mM KCl, 1.8 mM $CaCl_2$, 0.8 mM $MgCl_2$, 10 mM D-glucose, 10 mM HEPES, pH 7.4, 230 mosM. Patch pipettes were pulled from borosilicate glass and had resistances of 7–12 megaohms when filled with the internal solution (100 mM potassium gluconate, 0.1 mM $CaCl_2$, 5 mM $MgCl_2$, 1.1 mM EGTA, 10 mM HEPES, 3 mM Mg-ATP, 0.3 mM GTP, 3 mM phosphocreatine, pH 7.2, 215 mosM. IVM was dissolved in artificial cerebrospinal fluid containing 0.1% DMSO and preincubated with cultures at 37 °C/5% CO_2 for 15 min. All recordings were obtained at ambient temperature.

Data were analyzed using Clampfit version 9.2 software. Resting membrane potential was measured in the absence of injected current and corrected for the liquid junction potential at the electrode tip. To minimize the confounding effects of seal rupture during the transition to whole-cell configuration, cells with resting potentials of >-45 mV or seal resistances of <100 megaohms were omitted from analysis. The steady-state voltage response was plotted against the amount of current injected to measure a voltage-current (*V-I*) relationship. Total input resistance of the cell was determined from the slope of the linear portion of this relation, according to Ohm's law, $V = IR$. Input conductance was calculated as the inverse of resistance ($G = 1/r = I/V$). Evoked spikes were counted and plotted against the amount of injected current.

Immunofluorescent Labeling—Live neurons were immunolabeled without fixation using a published protocol (11). A V5 epitope tag including a linker sequence followed by a His_6 tag already encoded in the pcDNA3.1 vector was added to the C terminus of GluCl α and β subunits (-CASKGNSADIQHSGGRSSLEGPRFEGKPIPNPLLGLDSTRTGHHHHHH) by mutation of the stop codon (see above). The His_6 tag was not utilized. Surface receptors were labeled with primary mouse monoclonal anti-V5 antibody (1:200; catalog no. R960-25, Invitrogen) followed by a conjugated secondary Alexa Fluor 555 donkey anti-mouse antibody (1:400; catalog no. A-31570, Invitrogen). Antibodies were diluted into warm artificial cerebrospinal fluid and applied sequentially, incubating each for 30 min at 37 °C/5% CO_2 with appropriate rinse steps. Live cultures were imaged immediately after immunostaining.

Imaging—Living HEK293 cells and cultured neurons were imaged at 37 °C in a stage-mounted culture dish incubator (Warner Instruments). Transiently transfected HEK293 cells were imaged by TIRF microscopy, which enabled visualization of fluorescent receptors expressed in the plasma membrane and nearby intracellular vesicles (within 200 nm of the cell-coverslip interface). Prior to imaging, cell culture medium was replaced with phenol red-free CO_2-independent Leibovitz L-15 medium (catalog no. 21083-027, Invitrogen). TIRF images were obtained using an inverted microscope (Olympus IX81) with a 100×/1.45 numerical aperture Plan Apochromat oil objective. A stepping motor (T-cube stepper motor, Thorlabs) was used to control the position of the fiber optic and TIRF evanescent field illumination. A 488-nm laser was used to excite monomeric YFP fluorescence. Images were acquired using MetaMorph Premier software (Molecular Devices) at 16-bit resolution over 512 × 512 pixels and captured using a back-illuminated EMCCD camera (iXON DU-897) supported by ANDOR iQ2 software (Andor Technology).

Transiently transfected hippocampal neuron cultures were imaged using a laser-scanning confocal microscope (Nikon Eclipse C1si) equipped with a 63×/1.4 numerical aperture VC Plan Apochromat oil objective. Monomeric YFP fluorescence was acquired with 514-nm laser excitation. Alexa Fluor 555 and pDsRED2 (catalog no. 632409, Clontech) fluorescence was acquired with 561-nm laser excitation. Images were collected as *z*-stacks at a step size of 1.0 μm with 16-bit resolution over 512 × 512 pixels and a dwell time of 6.72 μs.

For confocal image analysis, the two different fluorescent signal intensities were correlated on a pixel-by-pixel basis using the Colocalization Colormap ImageJ plug-in (Adam Gorlewicz; available at the ImageJ web site). This software is based on a previously published algorithm (12). The correlation of a pair of pixels was calculated by the normalized mean deviation product (nMDP) as follows,

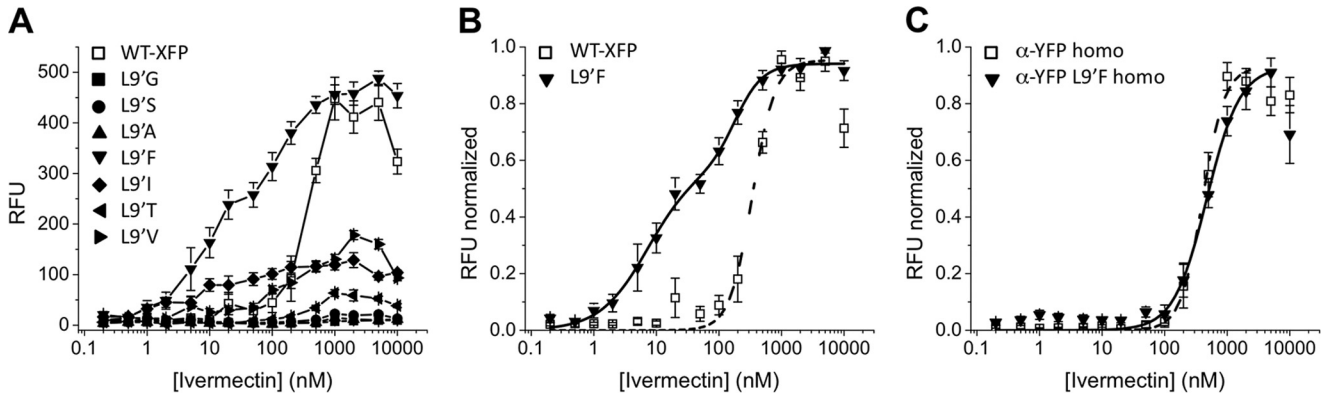

FIGURE 1. **Channel gating mutation L9′F increases IVM sensitivity of heteromeric GluCl.** *A*, concentration-response data for IVM activation of heteromeric GluCl WT-XFP and seven different leucine 9′ mutant receptors measured with a fluorescent membrane potential-sensitive dye. Response magnitudes are measured in relative fluorescence units (*RFU*). *B*, normalized IVM concentration-response relations for heteromeric GluCl WT-XFP and L9′F mutant receptors. The IVM concentration-response relation for the L9′F mutant was best fit by the sum of two Hill equations. *C*, normalized IVM concentration-response relations for WT-XFP and L9′F GluCl α homomers. Fitted parameters for IVM concentration-response relations are given in Table 1. *Error bars*, S.E.

$$\mathrm{nMDP}_{x,y} = \frac{(Ia - \overline{Ia})(Ib - \overline{Ib})}{(Ia_{\max} - \overline{Ia})(Ib_{\max} - \overline{Ib})} \qquad \text{(Eq. 1)}$$

where the intensity (I) for a given pixel in one image (a or b) is normalized to the average intensity and maximum intensity for that image. The nMDP values for each pixel range from −1 to 1 and are visualized on a *color scale* (see Figs. 7 and 8). Values <0 are represented by *cold colors* for exclusion of one fluorophore, and values >0 are shown in *hot colors*, indicating colocalization of both fluorophores. For the experimental conditions of the current study, the average of all positive (colocalized) nMDP values corresponds to total receptor surface expression, whereas the average number of perfectly correlated pixels (*i.e.* nMDP = 1) indicates the relative amounts of each subunit.

Statistics—Pooled data are shown as means ± S.E. Box plots represent the mean, median, 25th, and 75th percentiles. Statistical significance ($p < 0.05$) was determined by one-way analysis of variance on ranks using multiple pairwise comparison.

RESULTS

Gain-of-function Gating Mutation Increases Receptor Sensitivity to IVM—GluCl is a member of the Cys-loop superfamily of ligand-gated ion channels in which five individual subunits form homomeric or heteromeric receptor subtypes with varying functional properties. A number of studies on both cation-selective (nicotinic acetylcholine and serotonin 5-HT_3) and anion-selective (GABA and glycine) Cys-loop receptors have demonstrated that mutation of a highly conserved pore-lining residue, leucine 9′, to one of several other amino acids can dramatically increase agonist sensitivity through effects on channel gating (13–21). This gain-of-function effect is evident in the dose-response relation, in which channel activation occurs with lower concentrations of agonist.

To test GluCl receptors for increased IVM sensitivity, the highly conserved leucine 9′ residue in the M2 domain of the α subunit was mutated to one of seven other residues: L9′I, L9′F, L9′V, L9′A, L9′G, L9′S, or L9′T. Heteromeric GluCl αβ wild-type (WT-XFP) and leucine 9′ mutant channels (also XFP-tagged) were expressed in HEK293 cells and screened for receptor activation using a fluorescence-based assay with a membrane potential-sensitive dye. All mutants, except for L9′F, displayed reduced signals for IVM activation compared with WT-XFP (Fig. 1*A*). Weak agonist-induced signals were the result of elevated base-line fluorescence (data not shown), suggesting an increased level of background conductance, which has been reported for some leucine 9′ mutations in other Cys-loop receptors (13, 20, 22–25). The L9′F mutant retained a maximal response comparable with that of WT-XFP. Fitted IVM activation parameters for the normalized mean signal show a biphasic concentration-dependent relation for the L9′F mutant with an unambiguous increase in IVM sensitivity throughout the unsaturated concentration range compared with WT-XFP (Fig. 1*B* and Table 1). As a result, L9′F was designated as the best candidate mutation for increasing the sensitivity and preserving the amplitude of the ivermectin response.

The membrane potential-sensitive dye assay unexpectedly revealed that HEK293 cells expressing GluCl α homomers were indeed responsive to IVM (Fig. 1*C*), despite the failure of previous electrophysiological studies to detect IVM responses from α homomers expressed in mammalian cell lines (1, 2). GluCl α homomers containing the L9′F mutation were also responsive but did not show increased sensitivity to IVM (Table 1), implying that the gain-of-function effect of L9′F on IVM sensitivity requires co-assembly with the β subunit. GluCl β homomers were not responsive to applications of IVM.

Mutation of a Putative ER Retention Motif Enhances the High Sensitivity IVM Response—In the cell, multimeric membrane proteins are synthesized, matured, and assembled in the endoplasmic reticulum (ER) (26, 27). Proteins that are misfolded, unassembled, or improperly assembled are retained in the ER and ultimately targeted for ER-associated degradation (28, 29). This mechanism ensures that only properly assembled receptors are transported to the cell surface.

The amino acid sequence of a plasma membrane protein often contains specific signaling motifs to facilitate retention or export of the protein from the ER. The best characterized ER exit signals include D*X*E (30, 31), L*XX*(L/M)E (32), and (I/L)*X*M (33). These motifs exist on the cytosolic loops of a variety of membrane-associated proteins, where they are recognized by

TABLE 1

Fitted parameters for IVM concentration-response relations of WT and mutant GluCl receptors

Parameters correspond to IVM concentration-response relations in Figs. 2–4. The EC_{50} and Hill coefficient values represent the mean ± S.E. for the number of measurements (*n*) obtained. The relative fraction of the high sensitivity component (1st comp) for the biphasic relations is included.

GluCl channel	1st comp	EC_{50}	Hill	EC_{50}	Hill	*n*
		nM		nM		
α(WT) + β(WT)				107.14 ± 10.94	1.04 ± 0.09	12
α-YFP + β-YFP				302.08 ± 54.34	1.44 ± 0.27	12
α-YFP L9′F + β-YFP	0.61	7.27 ± 2.85	1.14 ± 0.24	185.35 ± 50.16	1.99 ± 0.82	6
α-YFP homomer				406.88 ± 21.08	2.47 ± 0.24	6
α-YFP L9′F homomer				472.67 ± 44.23	1.64 ± 0.19	6
α-YFP + β-YFP RSR_AAA	0.35	8.55 ± 3.16	2.50 ± 1.67	163.15 ± 38.31	2.04 ± 0.84	6
α-YFP + β-YFP RRR_AAA				111.88 ± 9.98	1.44 ± 0.16	6
α-YFP + β-YFP RSR_AAA/RRR_AAA				233.06 ± 17.71	1.44 ± 0.13	6
α-YFP L9′F + β-YFP RSR_AAA	0.53	3.91 ± 1.69	1.64 ± 0.69	95.28 ± 30.91	2.24 ± 1.27	12
α-YFP + β-YFP Y182F				380.41 ± 105.68	1.14 ± 0.24	6
α-YFP L9′F + β-YFP Y182F				159.81 ± 20.71	1.07 ± 0.12	6
α-YFP + β-YFP Y182F RSR_AAA				365.49 ± 48.35	1.35 ± 0.17	6
α-YFP L9′F + β-YFP Y182F RSR_AAA				45.08 ± 5.37	1.21 ± 0.14	6
α-mYFP + β-mYFP	0.29	3.58 ± 3.66	1.16 ± 0.80	170.46 ± 32.61	2.16 ± 0.79	6
α-mYFP L9′F + β-mYFP	0.49	1.35 ± 0.47	1.36 ± 0.85	185.58 ± 62.75	2.24 ± 1.65	6
α-mYFP L9′F + β-mYFP Y182F RSR_AAA	0.63	3.35 ± 1.36	1.04 ± 0.27	196.26 ± 49.81	2.50 ± 1.64	6

the primary cargo selection protein (Sec24) of the COPII-coated vesicles for transport from ER to Golgi. Well characterized ER retention signals include the classical C-terminal motifs, KDEL and KK*XX* (34, 35), and the cytosolic arginine-based signal, R*X*R (36). The R*X*R motif occurs in potassium channels (36), G-protein-coupled receptors (37), voltage-dependent Ca^{2+} channels (38), ionotropic glutamate receptors (39–41), and ionotropic Cys-loop receptors (42–44). Proteins containing the R*X*R motif are inferred to be retained in the ER (or maintained by COPI retrieval) until the retention signal is masked by multimeric assembly with other receptor subunits (45–47).

Fig. 2*A* notes putative ER signaling motifs in the amino acid sequences of GluCl α and β, in the large M3-M4 intracellular loop of each subunit. The α subunit contains a single putative ER export motif (LNLLE) immediately following the fluorescent fusion protein (XFP tags were inserted at restriction sites (3)). The β subunit contains two putative ER export motifs (LEM and DAE) and two putative ER retention motifs (RSR and RRR). The presence of putative retention motifs in β and their absence in α is consistent with the functional expression observed for these subunits in mammalian systems. For example, in the non-mammalian *Xenopus laevis* oocyte expression system, both α and β subunits form functional homomeric channels, of which α homomers are activated by IVM and β homomers are activated by glutamate (note that αβ heteromers can be activated by either glutamate or IVM) (48). In HEK293 cells, however, α homomer activation can be observed, but no agonist-induced response has successfully been detected for β homomers using either electrophysiology or fluorescence-based membrane potential assays (data not shown). This suggests that one or both of the retention motifs in the β subunit may prevent/limit its export to the plasma membrane in the absence of α subunits. Removal of ER retention signals could potentially allow for more uniform receptor expression and consistent neuronal silencing. To investigate this possibility, the putative ER retention motifs of the β subunit were mutated to alanine residues: GluCl β-YFP R318A/S319A/R320A for an "RSR_AAA" mutant and GluCl β-YFP R329A/R330A/R331A for an "RRR_AAA" mutant.

The mutant β subunits were co-expressed with α to produce heteromeric receptors in HEK293 cells and tested for IVM activation using the fluorescent membrane potential assay. The RSR_AAA and RRR_AAA mutant receptors as well as a double mutant receptor, RSR_AAA/RRR_AAA, produced IVM concentration-response relations similar to that of the WT-XFP receptor (Fig. 2*B* and Table 1). However, the RSR_AAA mutant displayed a distinct biphasic relation, suggesting the presence of an additional receptor population with high IVM sensitivity, presumably one with greater β subunit incorporation. The addition of the L9′F gain-of-function mutation to the RSR_AAA mutant receptor further enhanced the high sensitivity component of the IVM concentration-response relation. A comparison of peak amplitudes in response to 10 nM IVM indicated that the L9′F + RSR_AAA mutant receptor significantly increased receptor activation using lower concentrations of IVM (Fig. 2*C*). No IVM response was observed when mutant β subunits were expressed the in absence of the α subunit, implying that the removal of these putative retention motifs was not sufficient for surface expression of functional β homomers.

Addition of the Glutamate-insensitive Mutation Eliminates High IVM Sensitivity—To use this L9′F + RSR_AAA hyper-IVM-sensitive GluCl mutant receptor for pharmacogenetic silencing, sensitivity to the endogenous neurotransmitter glutamate had to be eliminated. Astonishingly, reintroduction of the glutamate binding site mutation Y182F in the β subunit abolished the high sensitivity component of the biphasic IVM concentration-response relation (Fig. 3*A*). The addition of the Y182F mutation to the singly mutated L9′F and RSR_AAA mutant receptors showed a similar effect (Fig. 3, *B* and *C*). Despite the loss of high IVM sensitivity, the Y182F mutation did suppress the glutamate sensitivity of the receptors (data not shown).

A Mutation That Prevents XFP Dimerization Restores High IVM Sensitivity—Fluorescent proteins tend to dimerize at high concentrations (49), but dimerization can also occur when XFPs are spatially restricted, such as when they are fused to membrane proteins (50). We suspected that XFP dimerization might interfere with IVM sensitivity because heteromeric WT-XFP receptors with YFP and CFP tags on either or both sub-

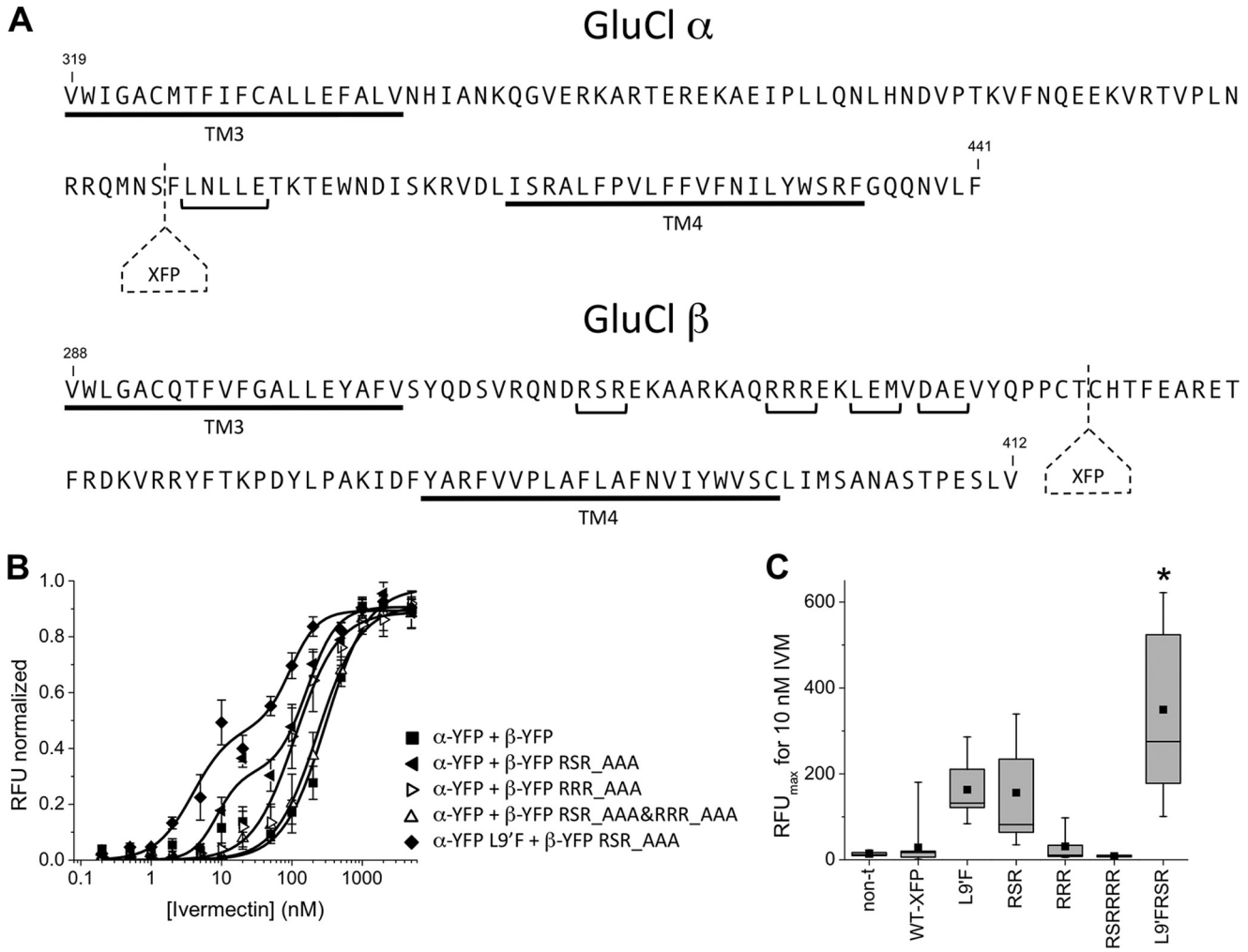

FIGURE 2. **Mutation of putative ER retention motif RSR also increases IVM sensitivity of heteromeric GluCl.** *A*, putative ER signaling motifs in GluCl α and β subunits. Amino acid sequences of the intracellular M3-M4 loop and flanking regions of GluCl α and β. The last amino acid of each sequence is the C-terminal residue. Transmembrane-spanning helices (M3 and M4) are *underlined*. The fluorescent protein (XFP) insertion point is denoted by *dashed lines*. The α subunit contains a single putative ER export motif (L*XX*(L/M)E). The β subunit contains two possible ER export motifs ((I/L)*XM* and D*X*E) and two potential ER retention motifs (R*X*R). *B*, normalized IVM concentration-response relations for heteromeric receptors containing RSR_AAA, RRR_AAA, and the double RSR_AAA/RRR_AAA mutations compared with WT-XFP. The RSR_AAA mutant produces a biphasic concentration-response relation. The addition of an L9′F mutation further enhances the high sensitivity component. *C*, the L9′F + RSR_AAA mutant receptor significantly increases the peak amplitude of the 10 nM IVM response relative to WT-XFP. IVM activation was measured using a fluorescent membrane potential assay. Fitted parameters for IVM concentration-response relations are given in Table 1. *Error bars*, S.E.

units all displayed IVM concentration-response relations that were right-shifted relative to the untagged WT receptor (Fig. 4*A*). The full data set for XFP-tagged and untagged subunits revealed that rightward shifts occurred only when the fluorescent protein was present in the α subunit (Fig. 4*B*). In further observations, the IVM concentration-response relation of the α-XFP homomer was also right-shifted relative to untagged α homomers (data not shown), again suggesting a loss of IVM sensitivity mediated by the fluorescent protein insertion.

Strictly monomeric XFPs (mXFPs) can be obtained by mutating the Ala-206 residue to Lys, a long, positively charged side chain that disrupts the hydrophobic dimer interface (51). Incorporating this mutation into the fluorescently tagged GluCl constructs prevented the rightward shift and even added a high sensitivity component to the IVM concentration-response relation of WT-mXFP (Fig. 4*C*). Including mXFP mutations in the heteromeric L9′F receptor produced a biphasic concentration-response relation more pronounced than any other previously obtained (Fig. 4*D*). More importantly, introducing mYFP into the initially favored L9′F + RSR_AAA receptor restored the high IVM sensitivity component that was lost upon the addition of the glutamate-insensitive Y182F mutation. This GluCl α-mXFP L9′F + β-mXFP Y182F RSR_AAA mutant receptor was more sensitive to IVM than GluClv1.0 by ~2 orders of magnitude (Fig. 4*E* and Table 1) while preserving insensitivity to physiologically relevant concentrations of glutamate (≤1 mM; Fig. 4, *F–H*) (52–54).

Biphasic Concentration-Response Relation Reflects Mixed Receptor Subunit Stoichiometries—In pentameric Cys-loop receptors, multicomponent concentration-response relations typically result when several subunit stoichiometries with differing agonist sensitivities are present in the receptor population (55–57). Variation in subunit stoichiometry may account for the biphasic IVM concentration-response relations observed for certain mutant GluCl subunit combinations. The α subunit L9′F mutation adds a high sensitivity component to

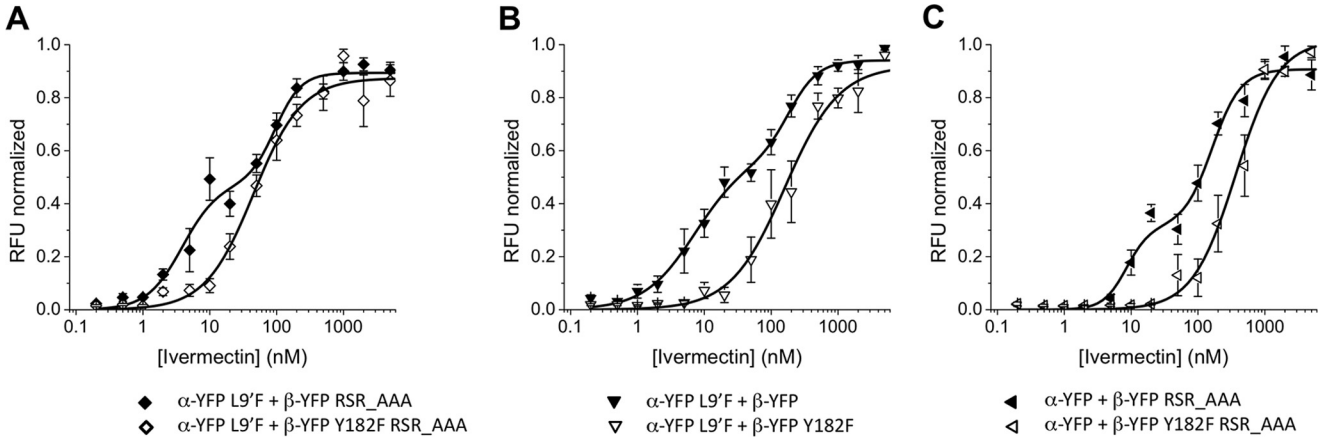

FIGURE 3. **Reintroduction of the glutamate-insensitive mutation eliminates mutant-induced increases in IVM sensitivity.** *A*, normalized IVM concentration-response relations show reintroduction of the Y182F mutation eliminates the high sensitivity component of the biphasic concentration dependence for the L9′F + RSR_AAA mutant receptor (from Fig. 2). *B* and *C*, the Y182F mutation similarly affected the concentration-response relations of the individual L9′F and RSR_AAA mutant receptors. IVM activation was measured using a fluorescent membrane potential assay. Fitted parameters for IVM concentration-response relations are given in Table 1. *Error bars*, S.E.

the IVM concentration-response relation only when co-expressed with the β subunit. Mutation of an ER retention sequence in the β subunit, which presumably increases the probability of β incorporation into the receptor, has a similar effect. Thus, the high IVM sensitivity component probably manifests from a shift in the ratio of α/β subunits in the assembled pentamer to include more β. To test this hypothesis, different ratios of α and β subunit DNA (1:1, 4:1, and 1:4) were transfected into HEK293 cells, and the IVM concentration-response relations were again measured using the fluorescent membrane potential assay. Consistent with our previous results, a 1:1 ratio produced a biphasic concentration-response relation. Biasing the ratio in favor of α (4:1) produced a decrease in IVM sensitivity, whereas biasing the ratio in favor of β (1:4), produced no further increase in IVM sensitivity (Fig. 5). Therefore, incorporation of the β subunit confers increased receptor sensitivity to IVM, but transfection of equal amounts of α and β subunit DNA appears to be optimal.

The fluorescent protein tags permit direct visualization and localization of GluCl subunits expressed in a cell. Images of HEK293 cells obtained by TIRF microscopy show that GluCl αβ heteromers and α homomers are expressed at the plasma membrane, but β homomers are not (Fig. 6, *A* and *B*). Specifically, the α-mYFP subunit shows plasma membrane fluorescence when transfected alone or cotransfected with untagged β. The β-mYFP subunit, on the other hand, shows plasma membrane fluorescence only when cotransfected with untagged α. Transfection of the β-mYFP subunit alone displays complete ER retention, as evidenced by the reticulated pattern of fluorescence and the lack of fluorescent filopodia at the periphery. GluCl β-mYFP subunits bearing the RSR_AAA, RRR_AAA, or the double RSR_AAA/RSR_AAA mutations display fluorescence patterns similar to the β-mYFP homomer (Fig. 6*C*). Thus, disruption of the putative ER retention motifs in the β subunit is not sufficient to allow plasma membrane expression of β homomers.

RSR Mutation Increases β Subunit Expression at the Plasma Membrane and the ER—The results above suggest that the ER retention mutation RSR_AAA enhances incorporation of the β subunit into heteropentameric GluCl receptors expressed on the cell surface. Although HEK293 cells were convenient for screening receptor function, primary neuronal cultures provide a more appropriate environment for investigating patterns of subunit expression. Preliminary confocal images of fluorescently tagged subunits transfected into embryonic rat hippocampal neurons displayed a deficient neuronal expression pattern for GluCl β homomers with minimal extension into the processes and comparatively few fluorescent neurons per imaging dish. GluCl α homomers and αβ heteromers, on the other hand, exhibit extensive fluorescent projections with no gross discernible differences (data not shown). Distinguishing between receptors retained in the ER and those expressed at the plasma membrane required colocalization markers.

Receptors expressed at the plasma membrane were targeted by live cell immunofluorescent surface staining. A V5 epitope tag was added to the extracellular C terminus of both α and β and subunits, which were then assayed for channel function in HEK293 cells to verify that pentameric assembly was not disrupted (data not shown). Cultured rat hippocampal neurons were then transfected with fluorescently tagged α and/or β subunits with one of the subunits containing the V5 epitope (*e.g.* α-mYFPV5 + β-mYFP). V5-tagged subunits expressed at the cell surface were detected by immunostaining with an anti-V5 primary antibody followed by a fluorescent Alexa Fluor 555-conjugated secondary antibody. Immediately after staining, the entire neuron was scanned for red and yellow fluorescence using confocal microscopy. Yellow fluorescence contributed by both subunits (mYFP) reflected total protein expression and was used to locate transfected neurons within the dish. Red fluorescence from live cell immunostaining (Alexa Fluor 555) emitted only from labeled subunits expressed at the cell surface. The extent of red and yellow fluorescent colocalization, therefore, served as a relative measure of surface expression, minimizing the effects of nonspecific antibody staining in our analysis. The fluorescence intensity correlation for each pixel was calculated by the nMDP and visualized on a *color scale* (Fig. 7*A*). Colocalization is evidenced by all positive nMDP values ($0 < x \leq 1$; shown in *hot colors*) and occurs only for receptors

	GluCl channel	EC_{50} (μM)	Hill	n
□	α(WT) + β(WT)	107.14 ± 10.94	1.04 ± 0.09	12
▲	α-YFP + β-CFP	365.20 ± 96.76	0.99 ± 0.16	12
▼	α-YFP + β-YFP	302.08 ± 54.34	1.44 ± 0.27	12
◀	α-CFP + β-YFP	249.59 ± 57.09	0.94 ± 0.15	6
▶	α-CFP + β-CFP	490.25 ± 39.35	1.89 ± 0.24	6
△	α(WT) + β-CFP	110.26 ± 13.09	0.96 ± 0.08	6
▽	α(WT) + β-YFP	123.85 ± 17.74	1.16 ± 0.15	6
◁	α-YFP + β(WT)	471.85 ± 35.39	1.58 ± 0.14	6
▷	α-CFP + β(WT)	255.72 ± 11.82	2.16 ± 0.17	6

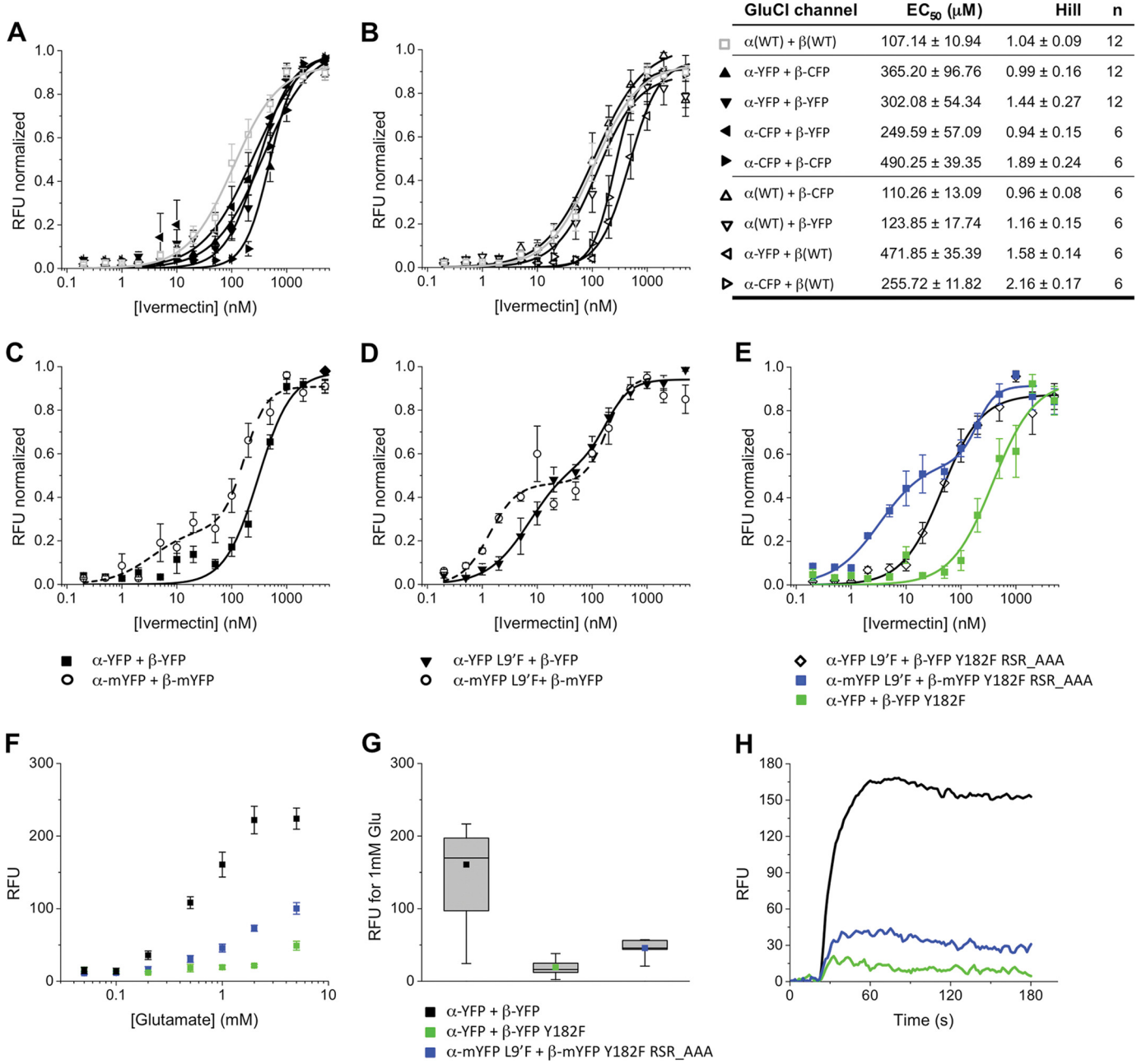

FIGURE 4. **Dimerization of the fluorescent protein (XFP) tags affects IVM sensitivity.** *A*, IVM concentration-response relations for heteromeric receptors with either YFP or CFP tags on both subunits are right-shifted compared with the untagged WT receptor. *B*, co-expression of tagged and untagged subunits reveals right-shifted relations particularly when the fluorescent protein is present on the α subunit. Fitted parameters for IVM concentration-response relations are given in the corresponding *table*. *C*, introduction of an mYFP mutation rectifies the rightward shift and adds a high sensitivity component. *D*, monomeric YFP also enhances the high IVM sensitivity component of the already biphasic L9′F concentration-response relation. *E*, finally, mYFP restores the high IVM sensitivity component lost upon the addition of the Y182F mutation to the L9′F + RSR_AAA receptor (from Fig. 3*A*). This newly engineered receptor (α-mXFP L9′F + β-mXFP Y182F RSR_AAA) is ~100-fold more sensitive to IVM than GluClv1.0. Fitted parameters for IVM concentration-response relations are given in Table 1. *F*, glutamate concentration-response relations for WT, GluClv1.0, and the revised receptor with the fluorescent membrane potential dye. *G*, the revised receptor retains insensitivity to physiologically relevant concentrations of glutamate (1 mM). *H*, sample fluorescent responses to 1 mM glutamate. *Error bars*, S.E.

expressed at the surface. Hence, greater nMDP values indicate a greater amount of GluCl expression at the plasma membrane.

The overall average of positive nMDP values provides a relative representation of total surface expression levels of receptor (note that the sum of all positive nMDP values is distorted by the size and number of cells imaged). Heteromeric WT receptors show the same level of total surface expression regardless of whether the V5 tag was on the α or β subunit (Fig. 7*B*). Homomeric receptors (transfected 1:1 with V5-tagged and untagged subunits for comparison with heteromers) corroborated the previous HEK293 cell observations that α homomers are expressed at the plasma membrane of neurons at levels comparable with αβ heteromers but that β homomers are not. Heteromeric receptors bearing the RSR_AAA retention mutation in the β subunit showed the same total surface expression levels as WT heteromers and α homomers, whereas those with

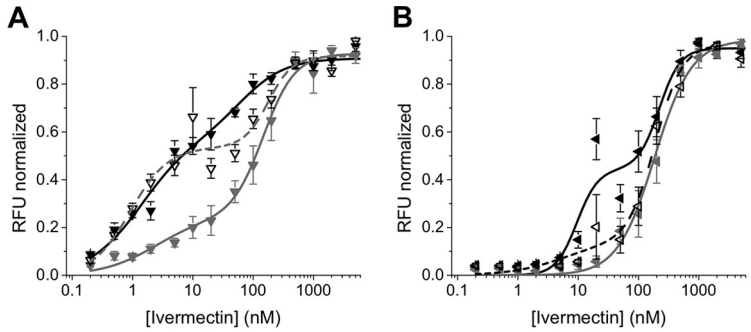

		1st comp	EC_{50} (μM)	Hill	EC_{50} (μM)	Hill	n
▼	α-mYFP L9′F + β-mYFP 1:1	0.64	1.37 ± 1.16	1.00 ± 0.40	65.16 ± 70.35	1.17 ± 0.86	6
▼	α-mYFP L9′F + β-mYFP 4:1	0.26	2.38 ± 2.64	1.00 ± 0.61	147.24 ± 27.16	1.66 ± 0.42	6
▽	α-mYFP L9′F + β-mYFP 1:4	0.58	0.92 ± 0.29	1.39 ± 0.56	178.36 ± 61.16	2.17 ± 1.51	6
◀	α-mYFP + β-mYFP RSR_AAA 1:1	0.47	9.56 ± 3.60	2.50 ± 1.90	220.21 ± 76.06	2.50 ± 2.03	6
◀	α-mYFP + β-mYFP RSR_AAA 4:1				184.22 ± 16.99	1.42 ± 0.15	6
◁	α-mYFP + β-mYFP RSR_AAA 1:4	0.15	5.58 ± 20.08	1.00 ± 1.64	188.88 ± 42.35	1.95 ± 0.78	6

FIGURE 5. **Biasing the subunit transfection ratio in favor of α suppresses the high sensitivity component of the biphasic IVM concentration-response relations.** Different ratios of α and β plasmid DNA (1:1, 4:1, and 1:4) were transfected into HEK293 cells. A 1:1 ratio (*black symbols*, *solid line*) produced the expected two-component concentration-dependent relationship for L9′F (*A*) and RSR_AAA (*B*) mutant receptors. Biasing in favor of the β subunit (1:4; *open symbols*, *dashed line*) does not further enhance IVM sensitivity. In contrast, biasing in favor of α (4:1; *gray symbols*, *solid line*) reduces IVM sensitivity. Fitted parameters for IVM concentration-response relations are given in the corresponding *table*. *Error bars*, S.E.

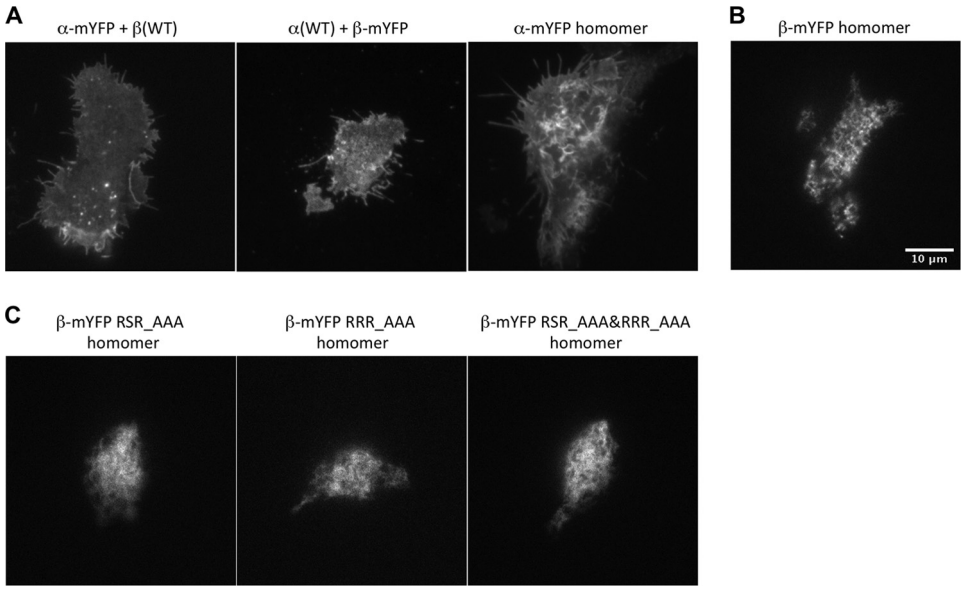

FIGURE 6. **Visualization of GluCl subunit expression in HEK293 cells.** *A*, TIRF images show fluorescent α and β subunits are expressed at the plasma membrane as heteromers. GluCl α homomers are also expressed at the plasma membrane. *B*, a reticulate pattern of fluorescence and the lack of hairlike filopodia at the periphery suggest that β homomers are exclusively retained in the ER. *C*, mutation of the putative ER retention motifs in the β subunit does not alter this pattern of fluorescence and therefore does not enable plasma membrane expression of β homomers.

the RRR_AAA and double RSR_AAA/RRR_AAA mutations in the β subunit resulted in lower surface expression levels.

Examining the number of maximally correlated pixels (nMDP = 1) within an image more directly represents surface expression levels of α *versus* β subunits. On average, the heteromeric WT, RRR_AAA, and RSR_AAA/RRR_AAA mutant receptors showed a greater number of maximally correlated pixels when the V5 tag was on the α subunit than on the β subunit, suggesting a greater number of α subunits present in the assembled pentamer (Fig. 7*C*). Heteromeric RSR_AAA mutant receptors, on the other hand, showed that maximal colocalization occurred more often for V5-tagged β than V5-tagged α, consistent with a shift in subunit stoichiometry. Altogether, the immunofluorescent results suggest that mutation of the putative RSR retention motif in the β subunit does not increase the total number of receptors trafficked to the plasma membrane but does increase the number of β subunits incorporated into assembled surface receptors.

To determine the relative amounts of WT and mutated β subunits remaining in the ER, colocalization analysis was per-

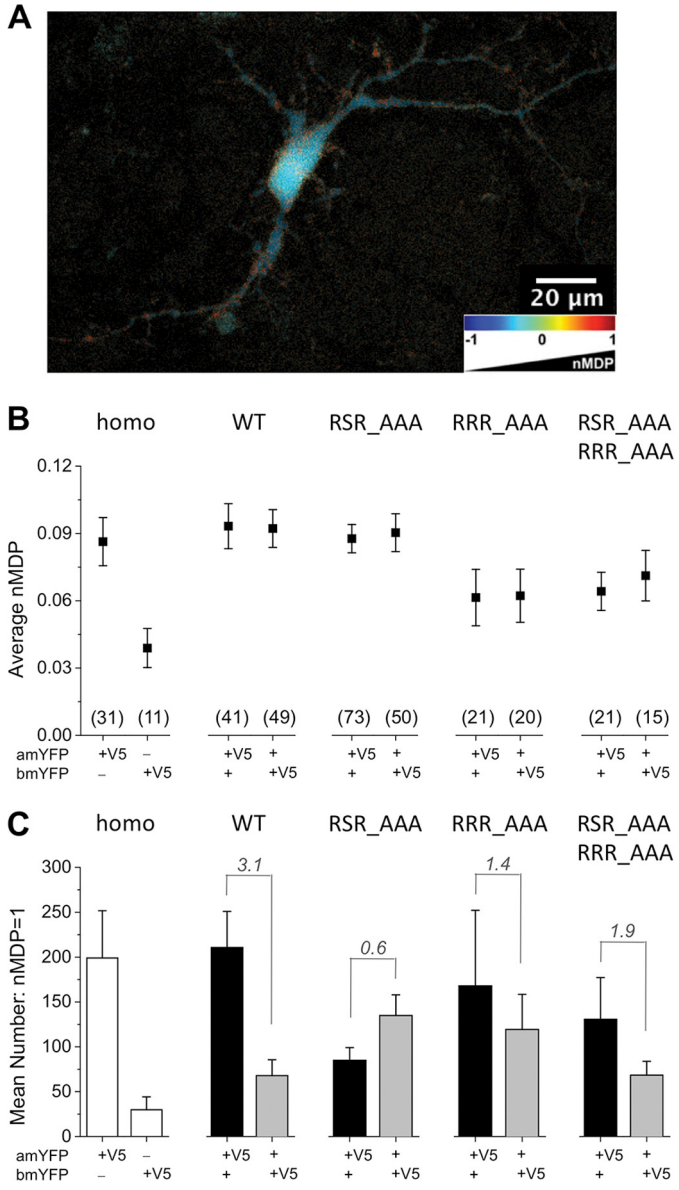

FIGURE 7. **The RSR_AAA mutation increases plasma membrane expression of the β subunit but not the total number of receptors.** *A*, confocal image example of colocalized Alexa Fluor 555 immunofluorescent surface staining and intrinsic mYFP fluorescence of GluCl α-mYFPV5 + β-mYFP viewed with the colocalization *color scale*. An nMDP correlation value is calculated for each pixel based on fluorescence intensity. *Hot colors* (nMDP > 0) denote colocalization and hence surface expression. *B*, the average of all positive nMDP values for a given receptor is representative of its total surface expression. GluCl α homomers are expressed at the plasma membrane, and β homomers are not. For heteromers, the same level surface expression was obtained regardless of whether the V5 tag was on the α or β subunit. Receptors bearing putative ER retention motif mutations do not increase total receptor surface expression compared with WT. *C*, the average number of pixels with nMDP values of unity indicates that more maximally correlated pixels occur with V5-tagged α than with V5-tagged β when WT, RRR_AAA, and RSR_AAA/RRR_AAA receptors are expressed as heteromers. In contrast, the RSR_AAA mutant receptor shows more maximal colocalization with V5-tagged β than with V5-tagged α, suggesting a shift in surface receptor subunit stoichiometry. *Error bars*, S.E.

formed on neurons cotransfected with non-fluorescent α subunits and the various mYFP-tagged β subunits together with the fluorescent ER marker dsRED (Fig. 8*A*). Once again, the RSR_AAA mutant differed significantly from WT and the RRR_AAA and RSR_AAA/RRR_AAA mutants, but rather than showing reduced ER localization, as would be presumed by relief of retention, the RSR_AAA mutant showed greater expression levels in the ER compared with the other β subunits (Fig. 8*B*). Because newly synthesized, improperly folded, or unassembled Cys-loop subunits remaining in the ER are known to be rapidly degraded (58–62), mutation of an ER retention motif could conceivably influence subunit degradation. These results may suggest that the RSR_AAA mutant β subunit is not being degraded as quickly, leaving more available for heteromeric assembly with α subunits.

An Improved Neuronal Silencing Tool—Rational mutation has led to a newly engineered GluCl receptor with increased sensitivity to IVM and improved expression of the β subunit. To determine whether this GluCl α-mXFP L9′F + β-mXFP Y182F RSR_AAA receptor is indeed an improved neuronal silencing tool over GluClv1.0, IVM-induced conductance and spike inhibition were measured from dissociated hippocampal neurons expressing these receptors (identified by fluorescence microscopy). Neurons were incubated with 0, 1, or 20 nM IVM for 15 min, rinsed with IVM-free saline, and then recorded in whole-cell current clamp mode for *V-I* relations using square current injection steps of −100 to 250 pA in 25-pA increments (Fig. 9*A*). The newly engineered receptor showed a significant increase in conductance (measured from the linear portion of the *V-I* relation; Fig. 9*C*) and a reduction in the mean evoked spike count (Fig. 9*B*) for both 1 and 20 nM IVM compared with GluClv1.0. Not only was spike suppression enhanced, the variability in spike suppression was also significantly reduced (Fig. 9*D*). Neither the presence of IVM nor receptor expression itself affected the resting membrane potential, confirming the integrity of induced spike inhibition (Fig. 9*E*). Thus, neuronal silencing achieved through IVM activation of the newly modified GluCl is indeed more sensitive and less variable than for GluClv1.0.

DISCUSSION

Previous *in vitro* and *in vivo* studies report that co-expression of both α and β subunits is required for GluCl-mediated neuronal silencing (1, 2). Variability in GluCl subunit expression (particularly that of the β subunit) appeared to be responsible for whether or not an individual neuron was inhibited by IVM. Our results show that functional, IVM-sensitive α homomers are actually expressed at the plasma membrane, but inclusion of the β subunit increases GluCl sensitivity to IVM. Therefore, variation in the proportion of heteromeric and homomeric receptors within individual neurons may account for the previously reported variation in IVM-induced spike suppression. We improved on the previous GluClv1.0 construct, introducing three new amino acid modifications. These modifications still do not provide a homogeneous receptor population, but, nevertheless, they generate a receptor population that is significantly more sensitive to IVM and that exhibits reduced variability in spike suppression. Therefore, this revised GluCl receptor, dubbed "GluClv2.0," should allow lower doses of IVM to be administered for *in vivo* silencing, alleviating concerns of side effects and suboptimal inhibition.

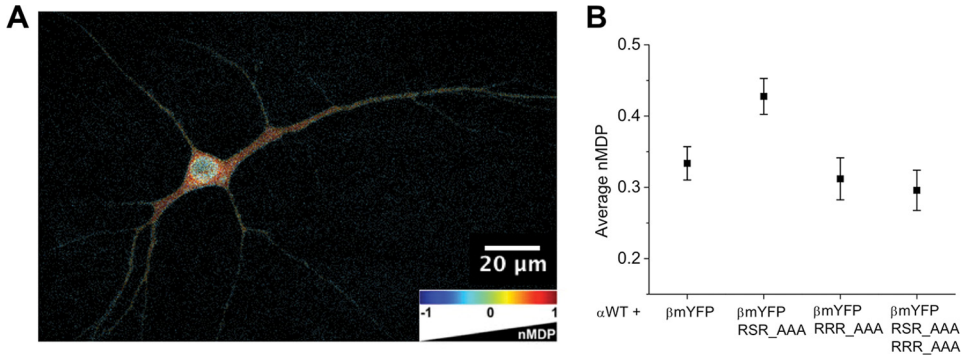

FIGURE 8. **The RSR_AAA mutation also increases β subunit expression in the ER.** *A*, confocal image of GluCl α(WT) + β-mYFP and the fluorescent ER marker dsRED viewed with the colocalization *color scale*. *B*, the average of all positive nMDP values represents the extent of β subunit localization in the ER. The RSR_AAA mutant subunit shows increased presence in the ER. *Error bars*, S.E.

Mechanisms of the Optimized Receptor—Concentration-response relations of GluCl α homomers and αβ heteromers bearing an L9′F mutation in the α subunit show that co-assembly with the β subunit significantly increases IVM sensitivity. The effects of biasing the stoichiometric ratio of transfected α and β subunits not only support this conclusion, they suggest that the L9′F mutation prefers or possibly promotes β subunit incorporation because biasing for α subunit expression with a 4:1 α/β subunit ratio still yields a biphasic IVM concentration-response relation for this mutant. Even the low sensitivity component of this relation is more sensitive (EC_{50} = 150 nM) than that of L9′F homomers (EC_{50} = 450 nM). Cys-loop receptor assembly (as described by one theory) involves an initial subunit dimerization step, followed by the dimerization of dimers and subsequent inclusion of a fifth subunit to form the final pentamer (63). The L9′F mutation may either promote α-β dimerization or hinder α-α dimerization, favoring the formation of a predominantly heteromeric αβ receptor population that includes more β subunits per assembled receptor.

According to conjecture, the arginine-based ER retention motif of the β subunit requires masking by co-assembly with the α subunit to exit the ER. This mechanism may explain the absence of β homomers at the plasma membrane. Our data show that removal of the retention motif (RSR_AAA) increases the amount of β exported to the plasma membrane in the presence of α. However, the RSR_AAA mutation also elevates β subunit levels in the ER, indicating that it does not simply enhance β subunit surface expression by reducing ER retention. Moreover, simply mutating the ER retention motif is not sufficient to allow surface expression of β homomers, suggesting that an additional unknown quality control mechanism is involved in β subunit retention. One possible explanation is that the RSR_AAA mutation impedes ER-associated degradation of the β subunit. It could do so either directly, prolonging its availability for α-β dimerization, or indirectly, by facilitating stable α-β dimer formation. A similar stabilizing effect within the ER appears to underlie nicotine-induced up-regulation of α4β2 nicotinic acetylcholine receptors to the plasma membrane (44). We do not know the extent to which the availability of β subunits in the ER impacts the propensity of α homomer formation. Limiting β subunit degradation may keep α homomer expression to a minimum.

The reason why reintroduction of the glutamate-insensitive mutation eliminated increased IVM sensitivity is less clear. The Y182F binding site mutation may reduce protein expression/stability of the β subunit or somehow inhibit α-β dimer formation. We cannot exclude the possibility that this mutation affects IVM activation of GluCl by interfering with the coupling between agonist binding and gating (64). However, restoration of the high sensitivity component of the IVM concentration-response relation by introducing the mYFP mutation suggests that it is more likely to be a consequence of altered subunit stoichiometry. The glutamate binding site is positioned at subunit interfaces where structural modifications could potentially disrupt heteromeric assembly. In this instance, the Y182F mutation would be preventing efficient pentameric incorporation of the β subunit, counteracting the benefits of the L9′F and RSR_AAA mutations.

Application of GluClv2.0—Since the initial proof-of-concept study, GluClv1.0 has been used in conjunction with channelrhodopsin-2-mediated activation to define an inhibitory microcircuit within the amygdala involved in mouse fear conditioning (65) and to identify a hypothalamic locus responsible for male mouse aggression and its close neuroanatomical relationship to mating circuits (66). In the former study, an intersectional approach was used to restrict GluCl expression to PKC-δ-containing GABAergic neurons in the central amygdala. Selective localization was achieved by targeted transgenic expression of GluCl α-CFP in all PKC-δ^+ neurons, followed by stereotaxic injection of an adeno-associated vector encoding GluCl β-YFP Y182F. Although GluCl/IVM-mediated silencing of PKC-δ^+ neurons yielded a significant enhancement of conditional freezing, the behavioral result was again confounded by a bimodal phenotype. Histological data revealed considerable variation in expression of the virally injected β subunit, reminiscent of the striatal proof-of-concept study. Interestingly, control animals transgenically expressing α alone were not affected by treatment with 10 mg/kg IVM, despite our present results indicating that α homomers are indeed expressed at the plasma membrane. Most likely, α homomer activation elicits insufficient Cl^- current to achieve neuronal silencing.

GluClv2.0 maintains the requirement of both α and β subunits for silencing. The pharmacokinetic properties of the silencing tool have not been altered. Another variant of IVM-

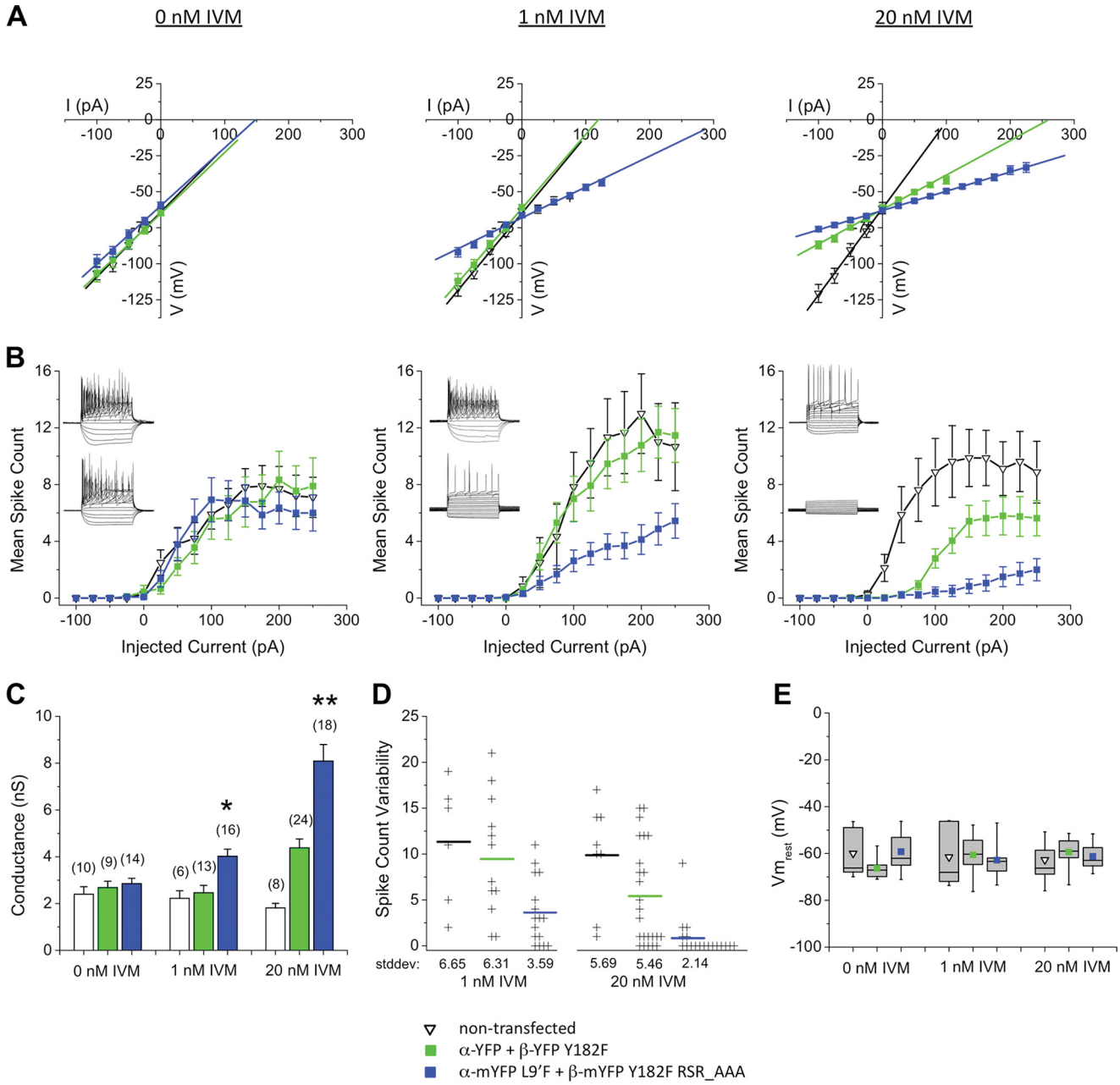

FIGURE 9. **An optimized neuronal silencing tool.** Action potential firing in response to depolarizing current pulses (−100 to 250 pA, 25-pA increments) was obtained from cultured hippocampal neurons in whole-cell current clamp mode following a 15-min preincubation with 0, 1, or 20 nM IVM. *A*, linear range of the *V-I* relations from neuronal cultures transfected with the revised construct (α-mYFP L9′F + β-mYFP Y182F RSR_AAA) was compared with those of GluClv1.0 (α-YFP + β-YFP Y182F) and non-transfected neurons. The revised receptor exhibits lower input resistance (as indicated by the slope) at 1 and 20 nM IVM. *B*, the revised receptor also reduced mean evoked spike counts at 1 and 20 nM IVM. *Insets*, voltage response to current injections for individual neurons expressing the original (*top*) and revised (*bottom*) receptors. *C*, the revised receptor induced a significant increase in conductance for both 1 and 20 nM IVM compared with GluClv1.0 (*, $p < 0.01$; **, $p < 0.001$). *D*, variability in evoked spike suppression, noted by the S.D. (*error bars*) of the spike count along the *abscissa*, is also significantly reduced with the revised receptor. *E*, neither construct expression nor the presence of IVM alone significantly altered the resting membrane potential (V_{mrest}).

induced silencing has been achieved by increasing the sensitivity of a mammalian homomeric glycine receptor (67), although this tool remains to be verified *in vivo*. In addition, an alternative Cys-loop orthogonal pharmacological silencing tool (based on chimeric nicotinic acetylcholine-glycine receptors of mammalian origins) capable of activating and inactivating on shorter time scales has recently been constructed (68). However, the cognate synthetic nicotinic agonist has demonstrated weak to moderate binding of other endogenous nicotinic acetylcholine receptors, and the absence of potential co-assembly of chimeric subunits with endogenous nicotinic acetylcholine receptors has not yet been verified. Even faster time-resolved neuronal silencing can be achieved using optogenetic techniques (69, 70), but this method is invasive and is not suitable for silencing large anatomical regions or diffuse signaling networks. The duration of light-induced manipulation is further limited by heat generation, which may alter neuronal activity or damage cell health (71). Thus, orthogonal phar-

macogenetic silencing using IVM activation of Cl^--permeable pentameric Cys-loop receptors remains a viable option for long term neuronal inhibition (such as that required in learning paradigms) and for assessing modulatory as opposed to regulatory roles in neuronal circuitry.

Acknowledgments—We thank Sheri McKinney for providing hippocampal neuron cultures. We also thank D. A. Dougherty and D. Anderson for comments.

REFERENCES

1. Lerchner, W., Xiao, C., Nashmi, R., Slimko, E. M., van Trigt, L., Lester, H. A., and Anderson, D. J. (2007) Reversible silencing of neuronal excitability in behaving mice by a genetically targeted, ivermectin-gated Cl^- channel. *Neuron* **54,** 35–49
2. Slimko, E. M., McKinney, S., Anderson, D. J., Davidson, N., and Lester, H. A. (2002) Selective electrical silencing of mammalian neurons *in vitro* by the use of invertebrate ligand-gated chloride channels. *J. Neurosci.* **22,** 7373–7379
3. Li, P., Slimko, E. M., and Lester, H. A. (2002) Selective elimination of glutamate activation and introduction of fluorescent proteins into a *Caenorhabditis elegans* chloride channel. *FEBS Lett.* **528,** 77–82
4. Slimko, E. M., and Lester, H. A. (2003) Codon optimization of *Caenorhabditis elegans* GluCl ion channel genes for mammalian cells dramatically improves expression levels. *J. Neurosci. Methods* **124,** 75–81
5. Burdett, E. C., Heckmann, R. A., and Ochoa, R. (1997) Evaluation of five treatment regimens and five diagnostic methods for murine mites (*Myocoptes musculinus* and *Myobia musculi*). *Contemp. Top. Lab. Anim. Sci.* **36,** 73–76
6. Adelsberger, H., Lepier, A., and Dudel, J. (2000) Activation of rat recombinant $\alpha_1\beta_2\gamma_{2S}$ $GABA_A$ receptor by the insecticide ivermectin. *Eur. J. Pharmacol.* **394,** 163–170
7. Khakh, B. S., Proctor, W. R., Dunwiddie, T. V., Labarca, C., and Lester, H. A. (1999) Allosteric control of gating and kinetics at $P2X_4$ receptor channels. *J. Neurosci.* **19,** 7289–7299
8. Krause, R. M., Buisson, B., Bertrand, S., Corringer, P. J., Galzi, J. L., Changeux, J. P., and Bertrand, D. (1998) Ivermectin. A positive allosteric effector of the α7 neuronal nicotinic acetylcholine receptor. *Mol. Pharmacol.* **53,** 283–294
9. Shan, Q., Haddrill, J. L., and Lynch, J. W. (2001) Ivermectin, an unconventional agonist of the glycine receptor chloride channel. *J. Biol. Chem.* **276,** 12556–12564
10. Li, Y. X., Zhang, Y., Lester, H. A., Schuman, E. M., and Davidson, N. (1998) Enhancement of neurotransmitter release induced by brain-derived neurotrophic factor in cultured hippocampal neurons. *J. Neurosci.* **18,** 10231–10240
11. Glynn, M. W., and McAllister, A. K. (2006) Immunocytochemistry and quantification of protein colocalization in cultured neurons. *Nat. Protoc.* **1,** 1287–1296
12. Jaskolski, F., Mulle, C., and Manzoni, O. J. (2005) An automated method to quantify and visualize colocalized fluorescent signals. *J. Neurosci. Methods* **146,** 42–49
13. Chang, Y., and Weiss, D. S. (1999) Allosteric activation mechanism of the $\alpha1\beta2\gamma2$ γ-aminobutyric acid type A receptor revealed by mutation of the conserved M2 leucine. *Biophys. J.* **77,** 2542–2551
14. Filatov, G. N., and White, M. M. (1995) The role of conserved leucines in the M2 domain of the acetylcholine receptor in channel gating. *Mol. Pharmacol.* **48,** 379–384
15. Kearney, P. C., Zhang, H., Zhong, W., Dougherty, D. A., and Lester, H. A. (1996) Determinants of nicotinic receptor gating in natural and unnatural side chain structures at the M2 9′ position. *Neuron* **17,** 1221–1229
16. Kosolapov, A. V., Filatov, G. N., and White, M. M. (2000) Acetylcholine receptor gating is influenced by the polarity of amino acids at position 9′ in the M2 domain. *J. Membr. Biol.* **174,** 191–197
17. Labarca, C., Nowak, M. W., Zhang, H., Tang, L., Deshpande, P., and Lester, H. A. (1995) Channel gating governed symmetrically by conserved leucine residues in the M2 domain of nicotinic receptors. *Nature* **376,** 514–516
18. Revah, F., Bertrand, D., Galzi, J. L., Devillers-Thiéry, A., Mulle, C., Hussy, N., Bertrand, S., Ballivet, M., and Changeux, J. P. (1991) Mutations in the channel domain alter desensitization of a neuronal nicotinic receptor. *Nature* **353,** 846–849
19. Shan, Q., Nevin, S. T., Haddrill, J. L., and Lynch, J. W. (2003) Asymmetric contribution of α and β subunits to the activation of $\alpha\beta$ heteromeric glycine receptors. *J. Neurochem.* **86,** 498–507
20. Thompson, S. A., Smith, M. Z., Wingrove, P. B., Whiting, P. J., and Wafford, K. A. (1999) Mutation at the putative $GABA_A$ ion-channel gate reveals changes in allosteric modulation. *Br. J. Pharmacol.* **127,** 1349–1358
21. Yakel, J. L., Lagrutta, A., Adelman, J. P., and North, R. A. (1993) Single amino acid substitution affects desensitization of the 5-hydroxytryptamine type 3 receptor expressed in *Xenopus* oocytes. *Proc. Natl. Acad. Sci. U.S.A.* **90,** 5030–5033
22. Bertrand, S., Devillers-Thiéry, A., Palma, E., Buisson, B., Edelstein, S. J., Corringer, P. J., Changeux, J. P., and Bertrand, D. (1997) Paradoxical allosteric effects of competitive inhibitors on neuronal α7 nicotinic receptor mutants. *Neuroreport* **8,** 3591–3596
23. Bianchi, M. T., and Macdonald, R. L. (2001) Mutation of the 9′ leucine in the $GABA_A$ receptor γ2L subunit produces an apparent decrease in desensitization by stabilizing open states without altering desensitized states. *Neuropharmacology* **41,** 737–744
24. Chang, Y., and Weiss, D. S. (1998) Substitutions of the highly conserved M2 leucine create spontaneously opening ρ1 γ-aminobutyric acid receptors. *Mol. Pharmacol.* **53,** 511–523
25. Pan, Z. H., Zhang, D., Zhang, X., and Lipton, S. A. (1997) Agonist-induced closure of constitutively open γ-aminobutyric acid channels with mutated M2 domains. *Proc. Natl. Acad. Sci. U.S.A.* **94,** 6490–6495
26. Ellgaard, L., and Helenius, A. (2003) Quality control in the endoplasmic reticulum. *Nat. Rev. Mol. Cell Biol.* **4,** 181–191
27. Teasdale, R. D., and Jackson, M. R. (1996) Signal-mediated sorting of membrane proteins between the endoplasmic reticulum and the Golgi apparatus. *Annu. Rev. Cell Dev. Biol.* **12,** 27–54
28. Hurtley, S. M., and Helenius, A. (1989) Protein oligomerization in the endoplasmic reticulum. *Annu. Rev. Cell Biol.* **5,** 277–307
29. Klausner, R. D., and Sitia, R. (1990) Protein degradation in the endoplasmic reticulum. *Cell* **62,** 611–614
30. Nishimura, N., and Balch, W. E. (1997) A di-acidic signal required for selective export from the endoplasmic reticulum. *Science* **277,** 556–558
31. Nishimura, N., Bannykh, S., Slabough, S., Matteson, J., Altschuler, Y., Hahn, K., and Balch, W. E. (1999) A di-acidic (DXE) code directs concentration of cargo during export from the endoplasmic reticulum. *J. Biol. Chem.* **274,** 15937–15946
32. Mossessova, E., Bickford, L. C., and Goldberg, J. (2003) SNARE selectivity of the COPII coat. *Cell* **114,** 483–495
33. Mancias, J. D., and Goldberg, J. (2008) Structural basis of cargo membrane protein discrimination by the human COPII coat machinery. *EMBO J.* **27,** 2918–2928
34. Jackson, M. R., Nilsson, T., and Peterson, P. A. (1990) Identification of a consensus motif for retention of transmembrane proteins in the endoplasmic reticulum. *EMBO J.* **9,** 3153–3162
35. Munro, S., and Pelham, H. R. (1987) A C-terminal signal prevents secretion of luminal ER proteins. *Cell* **48,** 899–907
36. Zerangue, N., Schwappach, B., Jan, Y. N., and Jan, L. Y. (1999) A new ER trafficking signal regulates the subunit stoichiometry of plasma membrane K_{ATP} channels. *Neuron* **22,** 537–548
37. Margeta-Mitrovic, M., Jan, Y. N., and Jan, L. Y. (2000) A trafficking checkpoint controls $GABA_B$ receptor heterodimerization. *Neuron* **27,** 97–106
38. Bichet, D., Cornet, V., Geib, S., Carlier, E., Volsen, S., Hoshi, T., Mori, Y., and De Waard, M. (2000) The I-II loop of the Ca^{2+} channel α1 subunit contains an endoplasmic reticulum retention signal antagonized by the β subunit. *Neuron* **25,** 177–190
39. Scott, D. B., Blanpied, T. A., Swanson, G. T., Zhang, C., and Ehlers, M. D. (2001) An NMDA receptor ER retention signal regulated by phosphorylation and alternative splicing. *J. Neurosci.* **21,** 3063–3072
40. Standley, S., Roche, K. W., McCallum, J., Sans, N., and Wenthold, R. J.

(2000) PDZ domain suppression of an ER retention signal in NMDA receptor NR1 splice variants. *Neuron* **28,** 887–898
41. Xia, H., Hornby, Z. D., and Malenka, R. C. (2001) An ER retention signal explains differences in surface expression of NMDA and AMPA receptor subunits. *Neuropharmacology* **41,** 714–723
42. Boyd, G. W., Doward, A. I., Kirkness, E. F., Millar, N. S., and Connolly, C. N. (2003) Cell surface expression of 5-hydroxytryptamine type 3 receptors is controlled by an endoplasmic reticulum retention signal. *J. Biol. Chem.* **278,** 27681–27687
43. Sadtler, S., Laube, B., Lashub, A., Nicke, A., Betz, H., and Schmalzing, G. (2003) A basic cluster determines topology of the cytoplasmic M3-M4 loop of the glycine receptor α1 subunit. *J. Biol. Chem.* **278,** 16782–16790
44. Srinivasan, R., Pantoja, R., Moss, F. J., Mackey, E. D., Son, C. D., Miwa, J., and Lester, H. A. (2011) Nicotine up-regulates $\alpha4\beta2$ nicotinic receptors and ER exit sites via stoichiometry-dependent chaperoning. *J. Gen. Physiol.* **137,** 59–79
45. Brock, C., Boudier, L., Maurel, D., Blahos, J., and Pin, J. P. (2005) Assembly-dependent surface targeting of the heterodimeric $GABA_B$ Receptor is controlled by COPI but not 14-3-3. *Mol. Biol. Cell* **16,** 5572–5578
46. Michelsen, K., Yuan, H., and Schwappach, B. (2005) Hide and run. Arginine-based endoplasmic-reticulum-sorting motifs in the assembly of heteromultimeric membrane proteins. *EMBO Rep*. **6,** 717–722
47. Yuan, H., Michelsen, K., and Schwappach, B. (2003) 14-3-3 dimers probe the assembly status of multimeric membrane proteins. *Curr. Biol.* **13,** 638–646
48. Cully, D. F., Vassilatis, D. K., Liu, K. K., Paress, P. S., Van der Ploeg, L. H., Schaeffer, J. M., and Arena, J. P. (1994) Cloning of an avermectin-sensitive glutamate-gated chloride channel from *Caenorhabditis elegans*. *Nature* **371,** 707–711
49. Yang, F., Moss, L. G., and Phillips, G. N., Jr. (1996) The molecular structure of green fluorescent protein. *Nat. Biotechnol.* **14,** 1246–1251
50. Zacharias, D. A. (2002) Sticky caveats in an otherwise glowing report. Oligomerizing fluorescent proteins and their use in cell biology. *Sci. STKE* **2002,** pe23
51. Zacharias, D. A., Violin, J. D., Newton, A. C., and Tsien, R. Y. (2002) Partitioning of lipid-modified monomeric GFPs into membrane microdomains of live cells. *Science* **296,** 913–916
52. Herman, M. A., and Jahr, C. E. (2007) Extracellular glutamate concentration in hippocampal slice. *J. Neurosci.* **27,** 9736–9741
53. Clements, J. D. (1996) Transmitter timecourse in the synaptic cleft. Its role in central synaptic function. *Trends Neurosci.* **19,** 163–171
54. Clements, J. D., Lester, R. A., Tong, G., Jahr, C. E., and Westbrook, G. L. (1992) The time course of glutamate in the synaptic cleft. *Science* **258,** 1498–1501
55. Moroni, M., and Bermudez, I. (2006) Stoichiometry and pharmacology of two human $\alpha4\beta2$ nicotinic receptor types. *J. Mol. Neurosci.* **30,** 95–96
56. Nelson, M. E., Kuryatov, A., Choi, C. H., Zhou, Y., and Lindstrom, J. (2003) Alternate stoichiometries of $\alpha4\beta2$ nicotinic acetylcholine receptors. *Mol. Pharmacol.* **63,** 332–341
57. Zhou, Y., Nelson, M. E., Kuryatov, A., Choi, C., Cooper, J., and Lindstrom, J. (2003) Human $\alpha4\beta2$ acetylcholine receptors formed from linked subunits. *J. Neurosci.* **23,** 9004–9015
58. Bonifacino, J. S., Cosson, P., Shah, N., and Klausner, R. D. (1991) Role of potentially charged transmembrane residues in targeting proteins for retention and degradation within the endoplasmic reticulum. *EMBO J.* **10,** 2783–2793
59. Bonifacino, J. S., and Lippincott-Schwartz, J. (1991) Degradation of proteins within the endoplasmic reticulum. *Curr. Opin. Cell Biol.* **3,** 592–600
60. Gorrie, G. H., Vallis, Y., Stephenson, A., Whitfield, J., Browning, B., Smart, T. G., and Moss, S. J. (1997) Assembly of $GABA_A$ receptors composed of $\alpha1$ and $\beta2$ subunits in both cultured neurons and fibroblasts. *J. Neurosci.* **17,** 6587–6596
61. Merlie, J. P., and Lindstrom, J. (1983) Assembly in vivo of mouse muscle acetylcholine receptor. Identification of an α subunit species that may be an assembly intermediate. *Cell* **34,** 747–757
62. Blount, P., and Merlie, J. P. (1990) Mutational analysis of muscle nicotinic acetylcholine receptor subunit assembly. *J. Cell Biol.* **111,** 2613–2622
63. Green, W. N. (1999) Ion channel assembly. Creating structures that function. *J. Gen. Physiol.* **113,** 163–170
64. Gleitsman, K. R., Shanata, J. A., Frazier, S. J., Lester, H. A., and Dougherty, D. A. (2009) Long-range coupling in an allosteric receptor revealed by mutant cycle analysis. *Biophys. J.* **96,** 3168–3178
65. Haubensak, W., Kunwar, P. S., Cai, H., Ciocchi, S., Wall, N. R., Ponnusamy, R., Biag, J., Dong, H. W., Deisseroth, K., Callaway, E. M., Fanselow, M. S., Lüthi, A., and Anderson, D. J. (2010) Genetic dissection of an amygdala microcircuit that gates conditioned fear. *Nature* **468,** 270–276
66. Lin, D., Boyle, M. P., Dollar, P., Lee, H., Lein, E. S., Perona, P., and Anderson, D. J. (2011) Functional identification of an aggression locus in the mouse hypothalamus. *Nature* **470,** 221–226
67. Lynagh, T., and Lynch, J. W. (2010) An improved ivermectin-activated chloride channel receptor for inhibiting electrical activity in defined neuronal populations. *J. Biol. Chem.* **285,** 14890–14897
68. Magnus, C. J., Lee, P. H., Atasoy, D., Su, H. H., Looger, L. L., and Sternson, S. M. (2011) Chemical and genetic engineering of selective ion channel-ligand interactions. *Science* **333,** 1292–1296
69. Gradinaru, V., Thompson, K. R., and Deisseroth, K. (2008) eNpHR. A *Natronomonas* halorhodopsin enhanced for optogenetic applications. *Brain Cell Biol.* **36,** 129–139
70. Zhang, F., Wang, L. P., Brauner, M., Liewald, J. F., Kay, K., Watzke, N., Wood, P. G., Bamberg, E., Nagel, G., Gottschalk, A., and Deisseroth, K. (2007) Multimodal fast optical interrogation of neural circuitry. *Nature* **446,** 633–639
71. Tye, K. M., and Deisseroth, K. (2012) Optogenetic investigation of neural circuits underlying brain disease in animal models. *Nat. Rev. Neurosci.* **13,** 251–266